Acta Crystallographica Section D
Biological Crystallography
ISSN 0907-4449

Structure of the Fab fragment from F124, a monoclonal antibody specific for hepatitis B surface antigen

F. A. Saul, B. Vulliez-le Normand, M. Passafiume, M.-M. Riottot and G. A. Bentley*

Unité d'Immunologie Structurale, CNRS URA 2185, Institut Pasteur, 25 Rue du Dr Roux, 75724 Paris, France

Correspondence e-mail: bentley@pasteur.fr

Received 9 February 2000
Accepted 1 June 2000

PDB Reference: F124 Fab fragment, 1f11.

The crystal structure of the Fab fragment from the monoclonal anti-preS2 antibody F124 (IgG1,κ) has been solved by molecular replacement and refined at 3.0 Å resolution. The Fab crystallizes with two independent molecules in the asymmetric unit. F124 recognizes an epitope contained within the preS2 segment between residues 120 and 132 of the surface antigen of hepatitis B virus. The antibody shows a high affinity for the glycan N-linked to Asn123, but it also cross-reacts with the non-glycosylated peptide fragment 120–132. Although crystallization was performed in the presence of an eightfold excess of the cross-reactive peptide, no evidence for the ligand was found in the antigen-binding site, which is close to a neighbouring molecule in the crystal lattice. The antigen-binding site has a groove-like topology which is modulated with pocket-like cavities. It is characterized by a large number of tyrosine and aspartate residues. The importance of germ-line mutations at the binding site is discussed.

1. Introduction

Hepatitis B surface antigen (HBsAg), comprising three distinct membrane-bound glycoproteins embedded in the external lipid envelope of hepatitis B virus (HBV), is highly immunogenic and can induce neutralizing antibodies (Ganem, 1996). Indeed, anti-HBsAg antibodies form the major component of the early humoral response to HBV (Neurath & Kent, 1988). The three proteins of HBsAg, designated S, M and L, are translated from different initiation sites within the same open reading frame of the viral genome. Thus, the proteins M and L share the same sequence as S (226 residues) in their C-terminal regions. The protein M, however, carries an additional 55 amino-acid segment, referred to as preS2 (conventional residue numbering 120–174), positioned N-terminal to the S sequence. The protein L in turn carries the preS1 segment of 108 or 119 residues, depending on viral subtype, in a position N-terminal to the M sequence. Although the three-dimensional structure of HBsAg is not known, the structure of the preS2 peptide segment 132–145 has been determined in recombinant forms of maltose-binding protein where this sequence was inserted at different permissive sites of the host protein (Saul *et al.*, 1997, 1998).

The anti-HBsAg monoclonal antibody F124 (isotype IgG1,κ), specific for the preS2 region of HBsAg, was obtained by immunizing mice with HBV particles of the *ay* subtype which were purified from a chronic carrier (Budkowska *et al.*, 1986). Binding of F124 to the preS2 peptide 120–145 is not compromised by the presence of F376, a monoclonal antibody specific for the region 132–145, suggesting that the epitope

Table 1
Crystal parameters and data-collection statistics for Fab F124.

Values for the highest resolution shell (3.11–3.00 Å) are given in parentheses.

Space group	*C*2
Unit-cell parameters	
a (Å)	135.7
b (Å)	54.0
c (Å)	120.0
β (°)	101.0
Z	8
V_m (Å^3 Da^{-1})	2.3
Resolution range (Å)	30.0–3.0
No. of unique reflections	17621 (1665)
Redundancy	1.9 (1.9)
Completeness (%)	99.2 (97.5)
$R_{\rm merge}$	13.1 (47.9)
Reflections with $I/\sigma(I) > 3$ (%)	59.4 (25.7)

Table 2
Molecular replacement.

All calculations were carried out with data in the 10–3.5 Å resolution range. Results for variable and constant dimer searches with the rotation function (R_v and R_c, respectively) and the single-body translation function (T_v and T_c, respectively) are shown as the peak height of the correct solution and the largest noise peak (given in parentheses). The peak heights correspond to the correlation coefficient as a percentage. In the rigid-body refinement, the variable and constant dimers were treated as independent components.

	Mol. 1	Mol. 2
R_v	21.5 (9.7)	18.4
R_c	20.4 (10.9)	12.7
T_v	18.0 (17.0)	17.6 (14.6)
T_c	18.9 (16.3)	16.9 (15.3)
Rigid-body refinement		
R factor (%)	39.6	
Correlation coefficient	57.4	

recognized by F124 is localized on the N-terminal region of preS2 (Budkowska *et al.*, 1987). Consistent with this observation, the epitope appears to include residue 126 of the preS2 region, as F124 has a lower affinity for the peptide 120–153 from the *adw2* serotype (Ala126) compared with the corresponding peptide of the *ayw* serotype (Thr126; Budkowska *et al.*, 1987). The epitope also includes the glycan N-linked to Asn123, as F124 has a significantly reduced affinity for subviral particles carrying S and M proteins after deglycosylation (Budkowska *et al.*, 1995). Thus, while the epitope recognized by F124 appears to be dominated by the carbohydrate component, cross-reactivity with the specific preS2 peptide 120–132 suggests that it also includes a region of polypeptide on the glycoprotein. In continuation of our study on the antigenic recognition by F124 (Passafiume *et al.*, 1998), we report here the crystal structure of the Fab fragment derived from this monoclonal antibody.

2. Experimental

2.1. Preparation and purification of Fab F124

The immunoglobulin was purified from ascitic fluid collected from BALB/c mice by precipitation with 40% ammonium sulfate followed by ion-exchange chromatography using a linear 0–500 m*M* NaCl gradient in Tris buffer pH 8.0 on a Mono Q column (Pharmacia). Two peaks corresponding to immunoglobulin were obtained, both of which showed identical recognition for recombinant particles bearing the preS and S domains (Michel *et al.*, 1984). The larger of these peaks was chosen for Fab preparation.

F124 fractions were pooled and dialysed across a Microsep 10K (Filtron) against 0.1 *M* potassium phosphate pH 7.2. After the addition of mercaptoethanol and EDTA to final concentrations of 14 and 12 m*M*, respectively, the protein solution was treated with papain (Boehringer) at an enzyme: substrate ratio of 1:50 for 2 h at 310 K. After incubating for 30 min at room temperature with 20 m*M* iodoacetamide, the buffer was changed to 0.02 *M* potassium phosphate pH 7.8. The protein was then applied to a DEAE–Sephacel (Pharmacia) column equilibrated with the same buffer. Upon addition of increasing concentrations of phosphate buffer to the column, Fab F124 was eluted at the 100 m*M* step. The Fab fragment was separated from the uncleaved IgG by gel-filtration chromatography (TSK G2000 SW, TosoHaas) and from another protein fragment (recognized by anti-Fc antibody) using an NaCl gradient in Tris buffer pH 8 on a Mono Q column.

2.2. Crystallization

In an attempt to form a complex between F124 and the peptide preS2(120–132), the ligand was added in an eightfold excess of concentration over that of the Fab and left to equilibrate for 5 h at 310 K. 2.5 µl protein solution was then mixed with 1 µl buffer containing 2 *M* ammonium sulfate, 0.1 *M* sodium acetate pH 4.6 and 5% PEG 400 (final protein concentration of 3.4 mg ml^{-1}). The resulting drop was sealed over a reservoir containing 1 ml of buffer in order to allow crystals to grow by vapour diffusion. Crystals took several months to appear and invariably grew in clusters from which it was difficult to separate monocrystalline fragments for diffraction measurements.

2.3. Data collection and processing

X-ray diffraction data were collected on a MAR345 imaging-plate detector system at the synchrotron beamline DW32, LURE (Orsay, France). Measurements were made with a single crystal of dimensions 0.2 × 0.1 × 0.03 mm at ambient temperature using an X-ray wavelength of 0.9607 Å. The crystal-to-detector distance was 250 mm and the active detector diameter was set to 180 mm. A total rotation range of 92° was covered in 1° steps, with each image being exposed for 300 s. Bragg intensities between the resolution limits of 30.0 and 3.0 Å were integrated and equivalent reflections were merged with the programs *HKL* and *SCALEPACK*, respectively (Otwinowski & Minor, 1997). Details of the crystal parameters and data-processing statistics are given in Table 1.

Table 3
Refinement statistics.

Values for the highest resolution shell (3.14–3.00 Å) are given in parentheses.

Number of protein atoms	6412
Number of solvent molecules	None
Average *B* factor	23.2
$F/\sigma(F)$ cut-off	0.0
Resolution range (Å)	30.0–3.0
No. of reflections	17621 (1991)
R factor	18.4 (27.1)
$R_{\rm free}$ (5% of data)	27.0 (34.8)
R.m.s. deviation, bond lengths (Å)	0.009
R.m.s. deviation, bond angles (°)	1.4
R.m.s. deviation, dihedral angles (°)	29.7
R.m.s. deviation, improper angles (°)	0.7

2.4. Molecular replacement

A preliminary model for the crystal structure of Fab 124 was obtained by molecular replacement using the program *AMoRe* (Navaza, 1994). The variable domain (including hypervariable regions) and constant domain dimers from the anti-digoxin antibody 26-10 (Jeffrey *et al.*, 1993; PDB entry 1igi) were used as independent search models in the rotation and translation functions. The rotation function gave clear indications for the orientation for the variable (V) and constant (C) dimers of the two independent molecules expected in the asymmetric unit. These orientations were used in turn for the translation function, in which the correct solution proved to be the highest peak in each case. Multi-body translation functions were then calculated to confirm the consistency of the independent solutions for the variable and constant dimers and to place these four components on a common crystallographic origin. Rigid-body refinement was subsequently performed to optimize the orientation and position of each independent dimer. The final model had structurally sensible pairings of the variable and constant dimers with no steric obstruction to the packing of the two independent Fab molecules in the unit cell, thus confirming the correctness of the solution. The two molecules are related by a non-crystallographic twofold axis which is approximately perpendicular to the *bc* crystal plane. Details of the molecular-replacement calculations are given in Table 2.

2.5. Refinement

Refinement was carried out with the program *X-PLOR* (Brünger *et al.*, 1987), with the geometrical parameters restrained to those proposed by Engh & Huber (1991). 95% of the data in the resolution range 30–3.0 Å was used to refine the structure, while the remaining 5% was used to check the course of refinement by calculating $R_{\rm free}$ (Brünger, 1992). Bulk-solvent corrections were applied according to the procedure described by Jiang & Brünger (1994). Individual temperature factors were restrained to target values by a 1.5 r.m.s. deviation for main-chain atoms and a 2.0 r.m.s. deviation for side chains. The initial model for refinement was the molecular-replacement solution based on the Fab 26-10 structure with complementarity-determining regions (CDRs) removed. Electron-density maps with Fourier coefficients $(2F_{\rm obs} - F_{\rm calc}, \alpha_{\rm calc})$ and $(F_{\rm obs} - F_{\rm calc}, \alpha_{\rm calc})$ were used to build the CDR and to manually adjust the atomic positions in other regions. Non-crystallographic symmetry (NCS) restraints were imposed on all atoms of the V and C dimers of the two crystallographically independent molecules. Weights for the positional NCS restraints were chosen to minimize the $R_{\rm free}$ factor. Map inspection and model building were carried out using the program *O* (Jones *et al.*, 1991). Refinement statistics are shown in Table 3.

3. Results and discussion

3.1. General description of the structure

Residue numbering and definitions of the CDR follow the conventions of Kabat *et al.* (1991). Residue numbers are preceded by L or H for the light and heavy chains, respectively. The Ramachandran plot is shown in Fig. 1. Electron density corresponding to the variable domains was continuous and well defined except for heavy-chain residues at positions 41 and 42. Certain regions within the constant domains had density that was too weak to reliably trace the polypeptide chain and were not included in the final model. These regions are residues 199–202 and beyond residue 212 in the Cκ domain and residues 128–136 and beyond residue 227 in the C_H1 domain. The structures of CDR-L1 and CDR-H3 are shown in Figs. 2(*a*) and 2(*b*), respectively, superimposed on the electron density. Although the Fab was crystallized in the presence of the preS2(120–132) peptide in an eightfold excess over the Fab

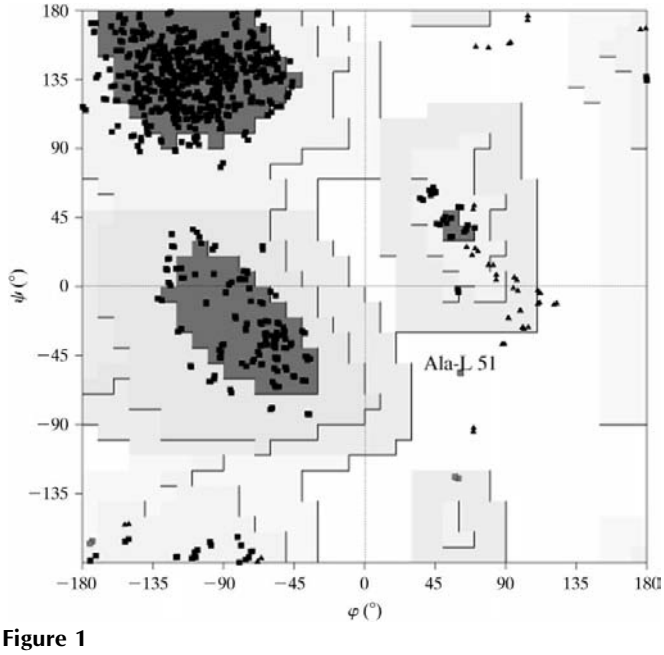

Figure 1
Ramachandran plot for the two independent molecules of Fab F124. A total of 83.6% of the non-glycine residues fall in the most favoured regions and 15.6% in the additional allowed region. AlaL51, which is in an unfavoured region, has dihedral angles that are characteristic of a γ-turn (Milner-White *et al.*, 1988). Residues in the unfavoured regions are labelled; glycines are shown as triangles. (Produced by the program *PROCHECK*; Laskowski *et al.*, 1993.)

Table 4
Close contacts (<3.5 Å) between the two molecules of FabF124 in the asymmetric unit with polar interactions indicated (*).

Molecule 1	Molecule 2	Distance
TyrL27D $C^{\varepsilon 2}$	AsnL92 O	3.3
TyrL27D OH	SerL91 O	2.7*
AspL28 N	AspL94 C^{γ}	3.4
AspL28 N	AspL94 $O^{\delta 1}$	3.0*
AspL28 N	AspL94 $O^{\delta 2}$	3.3*
AspL28 C^{γ}	AspH50 $O^{\delta 2}$	3.5
AspL28 $O^{\delta 1}$	TrpH46 $C^{\zeta 2}$	3.5
AspL28 $O^{\delta 1}$	AspH50 C^{β}	3.5
AspL28 $O^{\delta 1}$	AspH50 C^{γ}	3.3
AspL28 $O^{\delta 1}$	AspH50 $O^{\delta 2}$	3.5*
AspL28 $O^{\delta 2}$	AspH50 C^{γ}	3.4
AspL28 $O^{\delta 2}$	AspH50 $O^{\delta 2}$	2.8*
AspL30 $O^{\delta 2}$	TyrH33 OH	3.5*
SerL91 O	TyrL27D OH	2.9*
AspL94 C^{γ}	AspL28 N	3.5
AspL94 $O^{\delta 1}$	AspL28 N	3.0*
AspL94 $O^{\delta 2}$	AspL28 N	3.5*
PheL96 $C^{\varepsilon 1}$	TyrL27D $C^{\varepsilon 2}$	3.5
PheL96 $C^{\varepsilon 1}$	TyrL27D C^{ζ}	3.5
PheL96 $C^{\varepsilon 1}$	TyrL27D OH	3.4
TyrH33 $C^{\delta 2}$	AspL28 $O^{\delta 2}$	3.4
TyrH33 $C^{\varepsilon 2}$	AspL28 $O^{\delta 2}$	3.5
TyrH33 OH	AspL30 $O^{\delta 2}$	3.1*
TrpH47 $C^{\zeta 2}$	AspL28 $O^{\delta 1}$	3.4
AspH50 C^{β}	AspL28 $O^{\delta 1}$	3.4
AspH50 C^{γ}	AspL28 $O^{\delta 1}$	3.2
AspH50 $O^{\delta 2}$	AspL28 C^{γ}	3.3
AspH50 $O^{\delta 2}$	AspL32 $O^{\delta 1}$	3.2
AspH50 $O^{\delta 2}$	AspL32 $O^{\delta 2}$	2.8*

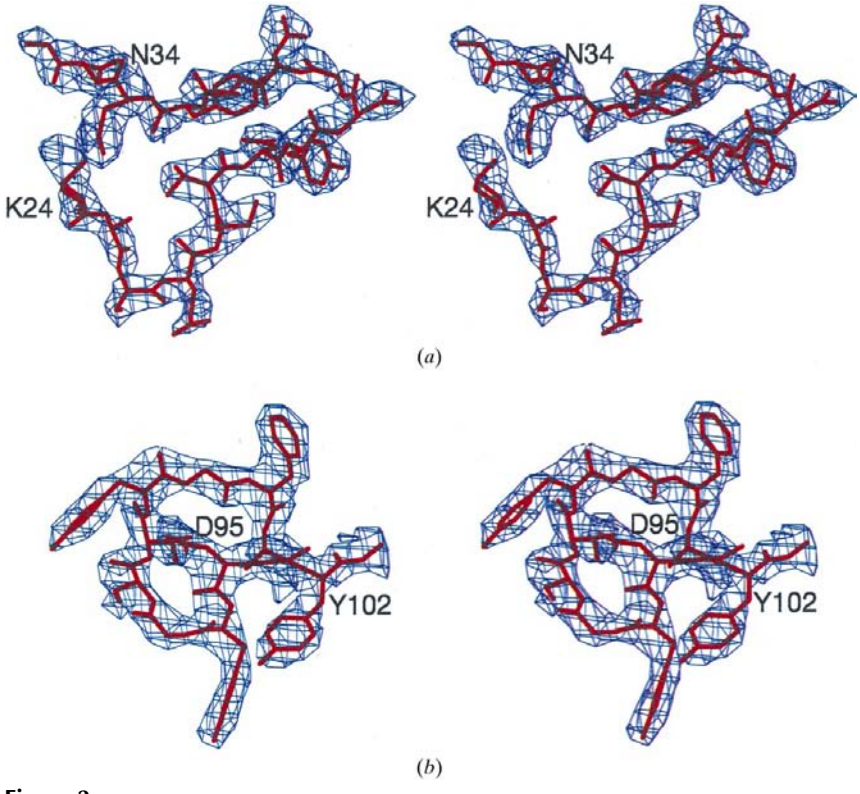

Figure 2
Stereoviews of the electron density: (*a*) CDR-L1 (LysL24–AsnL34) and (*b*) CDR-H3 (AspH95–TyrH102) of molecule 2. The maps were calculated with coefficients ($2F_{obs} - F_{calc}$, α_{calc}) and contoured at 1.2 r.m.s. deviation.

(see §2.2), no clear evidence for ligand could be found in the final electron-density maps in the vicinity of the antigen-binding site. Indeed, the close approach of the hypervariable regions (CDR-L1, CDR-L3, CDR-H1 and CDR-H2) of the two independent Fab molecules, shown in Table 4, precludes the presence of bound peptide at the antigen-binding site. These contacts reflect the non-crystallographic twofold symmetry relating the two molecules in the asymmetric unit to each other. The buried surface at the antigen-binding site is 385 Å^2, a value less than that observed for antibody–protein or antibody–peptide complexes (Stanfield & Wilson, 1995; Davies & Cohen, 1996). There is no evidence suggesting that significant dimerization of Fab fragments occurs in solution, as only a single peak was observed during purification by gel filtration.

Non-crystallographic symmetry was imposed on the V_L/V_H and C_L/C_H dimers of the two independent molecules during refinement (see §2.5), giving an r.m.s. difference of 0.24 Å for all restrained atoms. The elbow angle of Fab F124, defined by the angle subtended by the pseudo-dyads relating V_L to V_H and C_L to C_H, respectively, is 155° in both molecules. Packing of the molecules in the unit cell is shown in Fig. 3.

A comparison of the V_H domain of F124 with other immunoglobulin structures in the Protein Data Bank showed highest sequence and structural similarity with the anti-GD2 ganglioside Fab ME36.1 (Pichla *et al.*, 1997; PDB entry 1psk). Although encoded by different D and J_H genes, they have 94 of 119 residues identical (79%) and an r.m.s. difference of 1.33 Å between the C^{α} positions. For the region encoded by the V_H gene only (residues 1–94, which excludes CDR-H3) the r.m.s. difference is 0.74 Å. The V_L domain in turn shows highest sequence and structural similarity to the anti-HIV gp120 peptide antibody 58.2 (Stanfield *et al.*, 1999; PDB entry 3f58): 96 identical residues of 111 (86%) and 0.44 Å r.m.s. difference between their C^{α} positions.

3.2. Germ-line mutations

The nucleotide sequence of the genes coding for the V_H and V_L domains has been determined from cDNA that was synthesized from the mRNA isolated from F124-secreting hybridomas (Passafiume *et al.*, 1998). Sequence analysis showed that the V_L-coding region was derived from the Vκ21 germ-line gene and the Jκ4 segment. Six nucleotide changes with respect to Vκ21 are present (97.9% identity), but none in the region encoded by Jκ4. Two of these mutations are silent, while the four remaining changes lead to the amino-acid substitutions IleL2→Met in the first framework region (FR1), AlaL50→Val and GluL55→Lys in CDR-L2 and ArgL90→Gln in CDR-L3.

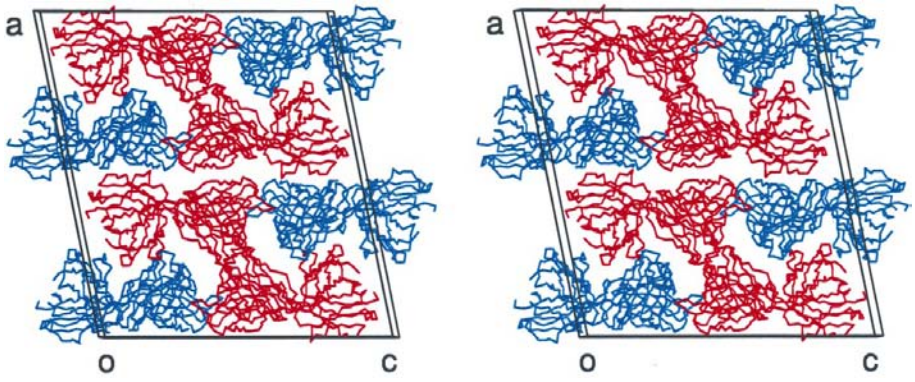

Figure 3
A stereoview showing the packing of the Fab fragments in the unit cell as seen along the *b* axis. The *a* and *c* axes and the origin (o) are indicated. The two independent molecules of Fab F124, related by a non-crystallographic twofold axis, are coloured red and blue, respectively. The molecules are represented as α-carbon skeletons.

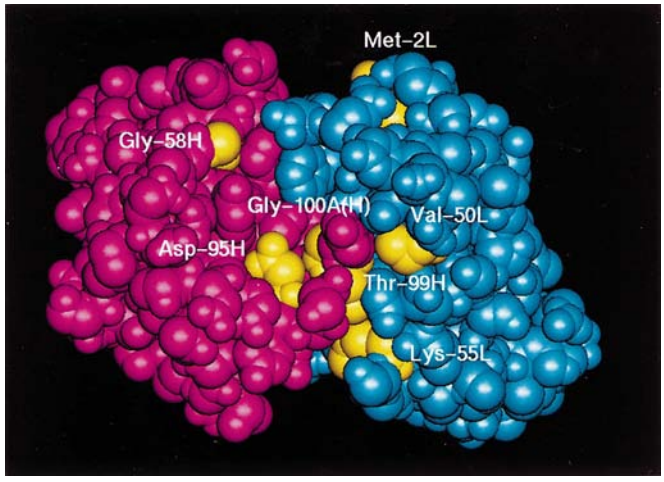

Figure 4
A view of the antigen-binding site showing residues that have mutated from the germ-line sequence. Mutated residues are shown in yellow; the remaining residues are shown in purple for V_H and blue for V_L

Although ValL50 and LysL55 are located in CDR-L2, they are prevented from making potential contacts with the antigen, as this hypervariable region is shielded from the binding site by CDR-L1 and CDR-H3, particularly by the aromatic residues TyrL27D, TyrL32 and TyrH100. Moreover, LysL55 falls outside the periphery of the usual antigen-contacting residues (MacCallum *et al.*, 1996). In this respect, it is interesting to note that CDR-L2 does not generally contribute to the antigen-binding site of anti-peptide antibodies (Stanfield & Wilson, 1995). The mutation ArgL90→Gln occurs in CDR-L3 but is buried and would thus not directly affect contacts with the antigen.

Searches with the F124 V_H sequence revealed no closely homologous germ-line V_H gene segment in the databases. Nonetheless, the variable heavy-chain domain is encoded by a V_H gene segment that shows 97.6% nucleotide sequence identity to that of M104E (J558 V_H gene family) and by the D and J gene segments DFL16.1 and JH3, respectively. Although M104E is a monoclonal antibody and thus is a product of somatic rearrangement and potential somatic hypermutation, its pattern of V_H-nucleotide differences with F124 and other closely related sequences found in the database search suggests that it is very close if not identical to a germ-line sequence. This assumption would seem reasonable as M104E belongs to the IgM isotype, which generally undergoes little if any hypermutation. Six nucleotide differences occur in V_H of F124 with respect to M104E, three of which are silent mutations. Of the other three differences, one is located in codon 58 (CDR-H2) and two in codon 94 (FR3), producing the amino-acid substitutions SerH58→Gly and ArgH94→Asn, respectively. GlyH58 is at the periphery of the antigen-binding site but appears to be well placed to make potential antigen contacts. AsnH94, which could have resulted from the joining of the V and D gene segments (Passafiume *et al.*, 1998), is the last framework residue before CDR-H3. Additional differences occur in the D and J segments at codons 95 (Asp), 99 (Thr) and 100A (Gly) and thus fall within CDR-H3. AspH95 is exposed at the centre of the antigen-binding site and is thus likely to be important for the specificity and affinity of F124. ThrH99, on the other hand, is partially buried and directed away from the binding site, while GlyH100A is completely buried. A view of the mutated residues is shown in Fig. 4.

3.3. The antigen-binding site

The CDRs of V_H and V_L conform to the canonical structure hypothesis put forward by Chothia and Lesk (Chothia & Lesk, 1987; Chothia *et al.*, 1989), *i.e.* that with the exception of CDR-H3, the structure of hypervariable loops can be described by a very limited number of possible main-chain conformations. Thus, for F124, CDR-H1 belongs to canonical structure 1, CDR-H2 to 2, CDR-L1 to 5, CDR-L2 to 1 and CDR-L3 to 1 (Chothia *et al.*, 1989, 1992; Martin & Thornton, 1996; Al-Lazikani *et al.*, 1997). CDR-H3 has ten residues and is thus slightly longer than the mean length of 8.7 for this hypervariable region in murine antibodies (Wu *et al.*, 1993).

The antigen-binding site of F124 takes the form of a groove running along the V_H/V_L interface, about 16 Å long by 10 Å wide and 8 Å deep, modulated by the presence of pocket-shaped cavities (Fig. 5). It is thus similar to certain other anti-saccharide antibodies of known three-dimensional structure: YsT9.1 (Evans *et al.*, 1994), BR96 (Jeffrey *et al.*, 1995) and ME36.1 (Pichla *et al.*, 1997). As already noted, the V_H domain of F124 and ME36.1 are closely related in sequence and structure. By contrast, Se155-4, an antibody directed against the O-antigen of *Salmonella*, possesses an antigen-binding site with a rather flat topology which includes a pocket 7 Å wide and 8 Å deep (Cygler *et al.*, 1991). The central depression of

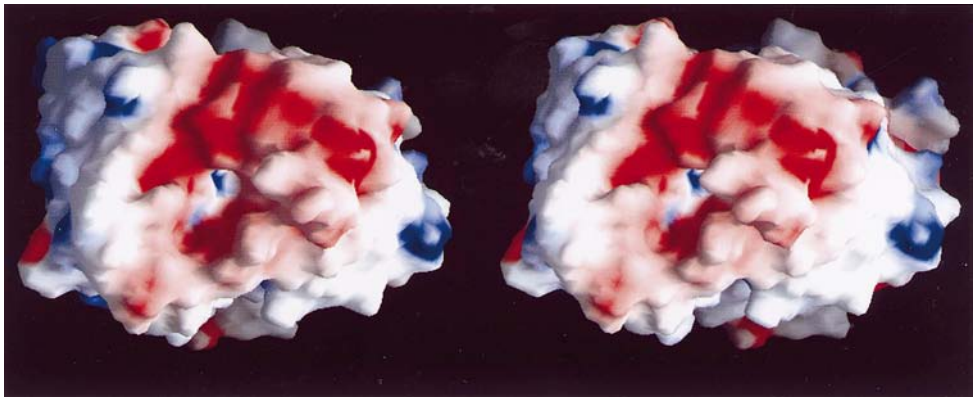

Figure 5
A stereoview of the antigen-binding site colour-coded for electrostatic potential; red represents positive and blue negative. (Prepared with the program *GRASP*; Nicholls *et al.*, 1991.)

the groove of F124 is lined with residues from CDR-L3 and CDR-H3. This is flanked by CDR-L1 (15 residues long) on one side and CDR-H1 (five residues) and CDR-H2 (four residues from 52A to 55 according to the definition by Chothia *et al.*, 1989) on the other.

The long hairpin turn of CDR-L1 (see Fig. 2*a*) has the same length as that found in the Fab crystal structures of 58.2 (PDB entries 1f58, 2f58 and 3f58), 59.1 (1acy, 1ai1), 50.1 (1ggb, 1ggc, 1ggi), F11.2.32 (1mf2, 2hrp), 40-50 (1ibg) and N10 (1nsn). The extremity of CDR-L1 in these structures shows variability of conformation from residues 27C–30, suggesting a certain degree of intrinsic flexibility in this long hypervariable loop. This flexibility can occur even for the same antibody in the free and complexed form, as with F11.2.32. Nonetheless, the conformation of CDR-L1 of F124 is close to that found in the peptide complexes of 58.2 (1f58, 2f58, 3f58), F11.2.32 (2hrp) and 59.1 (1acy, 1ai1).

Although only two of the residues affected by somatic rearrangement or hypermutation appear as likely candidates for direct interactions with the preS2 region of HBsAg (GlyH58 and AspH95), the others (with the exception of MetL2) could modulate CDR main-chain conformation and thus indirectly affect the disposition of the antigen-contacting regions. The antigen-binding site is lined with a number of acidic residues (AspL27C, AspL28, AspL30, AspL94, AspH50, AspH95) and aromatic residues (TyrL27D, TyrL32, PheL96, TyrH32, TyrH33, TyrH100) located in the hypervariable regions. In particular, tyrosine side chains from L27D, L32 and H100 form a contiguous aromatic patch. The framework residue TrpH47 is also partially exposed in the antigen-binding site.

4. Conclusions

The anti-preS2 monoclonal antibody F124 conforms to the suggestion that the antigen-binding sites of anti-saccharide antibodies generally adopt a groove- or pocket-type topology (Cisar *et al.*, 1975; Padlan & Kabat, 1991). To date, only the structures of Fab Se155-4 and Fab BR96 have been reported as complexes with their carbohydrate ligand. In both cases, aromatic residues in the antigen-binding site do not interact hydrophobically with the hexose rings of the ligand to the same extent as found in other protein–carbohydrate complexes (Vyas, 1991), but rather are involved in hydrogen bonding in the case of tryptophan and tyrosine. Certain ones of the five tyrosine residues present in the antigen-binding site of F124 may thus interact with the glycan component of the preS2 epitope in this manner.

Peptide fragments containing the preS2(120–132) sequence successfully compete with the native antigen for recognition by F124; however, the detailed contribution of the protein component of HBsAg in binding to the antibody has yet to be determined. Although Fab F124 was crystallized in the presence of the peptide preS2(120–132), no clear evidence for it could be found in the electron-density maps. The absence of ligand in the crystals could indicate that the binding energy between Fab molecules in the lattice is larger than the binding energy between the Fab and the peptide preS2(120–132), causing its displacement during crystallization. A continued search for alternative crystallization conditions for a potential Fab–antigen complex is under way.

We thank the staff of LURE, Orsay for providing measuring facilities and assistance at the synchrotron source. This research was supported by funds from the Institut Pasteur, the Centre National de la Recherche Scientifique, the Association pour la Recherche sur le Cancer and the Ligue Nationale contre le Cancer.

References

Al-Lazikani, B., Lesk, A. M. & Chothia, C. (1997). *J. Mol. Biol.* **273**, 927–948.
Brünger, A. T. (1992). *Nature (London)*, **355**, 472–475.
Brünger, A. T., Kuriyan, J. & Karplus, M. (1987). *Science*, **235**, 458–460.
Budkowska, A., Bedossa, P., Groh, F., Louise, A. & Pillot, J. (1995). *J. Virol.* **69**, 840–848.
Budkowska, A., Dubreuil, P., Riottot, M.-M., Braintais, M.-J. & Pillot, J. (1987). *J. Immunol. Methods*, **97**, 77–85.
Budkowska, A., Riottot, M.-M., Dubreuil, P., Lazizi, Y., Brechot, C., Sobczak, E., Petit, M.-A. & Pillot, J. (1986). *J. Med. Virol.* **20**, 111–125.
Chothia, C. & Lesk, A. M. (1987). *J. Mol. Biol.* **196**, 901–917.
Chothia, C., Lesk, A. M., Gherardi, E., Tomlinson, I. M., Walter, G., Marks, J. D., Llewelyn, M. B. & Winter, G. (1992). *J. Mol. Biol.* **227**, 799–817.
Chothia, C., Lesk, A. M., Tramontano, A., Lewit, M., Smith-Gill, S. J., Air, G., Sheriff, S., Padlan, E. A., Davies, D., Tulip, W. R., Colman, P. M., Spinelli, S., Alzari, P. M. & Poljak, R. J. (1989). *Nature (London)*, **342**, 877–883.

Cisar, J., Kabat, E. A., Dorner, M. M. & Liao, J. (1975). *J. Exp. Med.* **142**, 435–459.
Cygler, M., Rose, D. R. & Bundle, D. R. (1991). *Science*, **253**, 442–445.
Davies, D. R. & Cohen, G. H. (1996). *Proc. Natl Acad. Sci. USA*, **93**, 7–12.
Engh, R. A. & Huber, R. (1991). *Acta Cryst.* A**47**, 392–400.
Evans, S. V., Rose, D. R., To, R., Young, N. M. & Bundle, D. R. (1994). *J. Mol. Biol.* **241**, 691–705.
Ganem, D. (1996). *Fields' Virology*, edited by B. N. Fields & D. M. Knipe, pp. 2703–2737. Philadelphia: Lippencott–Raven.
Jeffrey, P. D., Bajorath, J., Chang, C. Y., Yelton, D., Hellström, I. & Sheriff, S. (1995). *Nature Struct. Biol.* **2**, 466–471.
Jeffrey, P. D., Strong, R. K., Sieker, L. C., Chang, C. Y., Campbell, R. L., Petsko, G. A., Haber, E., Margolies, M. N. & Sheriff, S. (1993). *Proc. Natl Acad. Sci. USA*, **90**, 10310–10314.
Jiang, J. S. & Brünger, A. T. (1994). *J. Mol. Biol.* **243**, 100–115.
Jones, T. A., Zou, J. Y., Cowan, S. W. & Kjeldgaard, M. (1991). *Acta Cryst.* A**47**, 110–119.
Kabat, E. A., Wu, T. T., Perry, H. M., Gottesman, K. S. & Foeller, C. (1991). In *Sequences of Proteins of Immunological Interest*, 3rd ed. Bethesda, MD: US Department of Health and Human Services, NIH.
Laskowski, R. A., McArthur, M. W., Moss, D. S. & Thornton, J. M. (1993). *J. Appl. Cryst.* **26**, 283–291.
MacCallum, R. M., Martin, A. C. R. & Thornton, J. M. (1996). *J. Mol. Biol.* **262**, 732–745.
Martin, A. C. R. & Thornton, J. M. (1996). *J. Mol. Biol.* **263**, 800–815.
Michel, M.-L., Pontisso, P., Sobczak, E., Malpièce, Y., Steek, R. F. & Tiollais, P. (1984). *Proc. Natl Acad. Sci. USA*, **81**, 7708–7712.
Milner-White, E. J., Ross, B. M., Ismail, R., Belhady-Mostefa, K. & Poet, R. (1988). *J. Mol. Biol.* **204**, 777–782.
Navaza, J. (1994). *Acta Cryst.* A**50**, 157–163.
Neurath, A. R. & Kent, S. B. H (1988). *Adv. Virus Res.* **34**, 65–142.
Nicholls, A., Sharp, K. A. & Honig, B. (1991). *Proteins Struct. Funct. Genet.* **11**, 281–296.
Otwinowski, Z. & Minor, W. (1997). *Methods Enzymol.* **276**, 307–326.
Padlan, E. A. & Kabat, E. A. (1991). *Methods Enzymol.* **203**, 3–21.
Passafiume, M., Vulliez-le Normand, B., Riottot, M.-M. & Bentley, G. A. (1998). *FEBS Lett.* **441**, 407–412.
Pichla, S. L., Murali, R. & Burnett, R. M. (1997). *J. Struct. Biol.* **119**, 6–16.
Saul, F. A., Vulliez-le Normand, B., Lema, F. & Bentley, G. A. (1997). *Proteins Struct. Funct. Genet.* **27**, 1–8.
Saul, F. A., Vulliez-le Normand, B., Lema, F. & Bentley, G. A. (1998). *J. Mol. Biol.* **280**, 185–192.
Stanfield, R. L., Cabezas, E., Satterthwait, A. C., Stura, E. A., Profy, A. T. & Wilson, I. A. (1999). *Struct. Fold. Des.* **7**, 131–142.
Stanfield, R. L. & Wilson, I. A. (1995). *Curr. Opin. Struct. Biol.* **5**, 103–113.
Vyas, N. K. (1991). *Curr. Opin. Struct. Biol.* **1**, 732–740.
Wu, T. T., Johnson, G. & Kabat, E. A. (1993). *Proteins Struct. Funct. Genet.* **16**, 1–7.